HHS Public Access

Author manuscript

Cancer Res. Author manuscript; available in PMC 2019 March 25.

Published in final edited form as:

Cancer Res. 2019 March 15; 79(6): 1214–1225. doi:10.1158/0008-5472.CAN-18-1127.

Dynamics of tumor and immune responses during immune checkpoint blockade in non-small cell lung cancer

Valsamo Anagnostou[1,2,#,*], **Patrick M. Forde**[1,2,*], **James R. White**[1], **Noushin Niknafs**[1], **Carolyn Hruban**[1], **Jarushka Naidoo**[1,2], **Kristen Marrone**[1,2], **I.K. Ashok Sivakumar**[1,3,4], **Daniel C. Bruhm**[1], **Samuel Rosner**[5], **Jillian Phallen**[1], **Alessandro Leal**[1], **Vilmos Adleff**[1], **Kellie N. Smith**[1,2], **Tricia R. Cottrell**[1,6], **Lamia Rhymee**[1], **Doreen N. Palsgrove**[1], **Christine L. Hann**[1], **Benjamin Levy**[1], **Josephine Feliciano**[1], **Christos Georgiades**[7], **Franco Verde**[7], **Peter Illei**[1,2,6], **Qing Kay Li**[1,6], **Edward Gabrielson**[1,6], **Malcolm V. Brock**[8], **James M. Isbell**[9], **Jennifer L. Sauter**[10], **Janis Taube**[1,2,6], **Robert B. Scharpf**[1], **Rachel Karchin**[1,3], **Drew M. Pardoll**[1,2], **Jamie E. Chaft**[11], **Matthew D. Hellmann**[11], **Julie R. Brahmer**[1,2], and **Victor E. Velculescu**[1,2,3,#]

[1]The Sidney Kimmel Comprehensive Cancer Center, Johns Hopkins University School of Medicine, Baltimore, MD 21287, USA

[2]The Bloomberg-Kimmel Institute for Cancer Immunotherapy, Johns Hopkins University School of Medicine, Baltimore, MD 21287, USA

[3]Institute for Computational Medicine, Johns Hopkins University, Baltimore, MD 21204, USA.

[4]Applied Physics Laboratory, Laurel, MD 20723, USA

[5]Department of Internal Medicine, Johns Hopkins Bayview Medical Center, Baltimore, MD 21224, USA

[6]Department of Pathology, Johns Hopkins University School of Medicine, Baltimore, MD 21287, USA

[7]Department of Radiology, Johns Hopkins University School of Medicine, Baltimore, MD 21287, USA

[8]Department of Surgery, Johns Hopkins University School of Medicine, Baltimore, MD 21287, USA

[9]Thoracic Service, Department of Surgery, Memorial Sloan Kettering Cancer Center, New York, New York, NY 10065, USA.

[10]Department of Pathology, Memorial Sloan Kettering Cancer Center, New York, NY 10065, USA.

[11]Thoracic Oncology Service, Department of Medicine, Memorial Sloan Kettering Cancer Center and Weill Cornell Medical College, New York, NY 10065, USA

[#]**Corresponding authors:** Valsamo Anagnostou, M.D., Ph.D., The Sidney Kimmel Comprehensive Cancer Center, Johns Hopkins University School of Medicine, 1550 Orleans St, Rm 554, Baltimore, MD 21287, Phone: (410) 614-8948, vanagno1@jhmi.edu, Victor Velculescu, M.D., Ph.D., The Sidney Kimmel Comprehensive Cancer Center, Johns Hopkins University School of Medicine, 1550 Orleans St, Rm 544, Baltimore, MD 21287, Phone: (410) 955-7033, velculescu@jhmi.edu.

[*]These authors contributed equally to this work.

Abstract

Despite the initial successes of immunotherapy, there is an urgent clinical need for molecular assays that identify patients more likely to respond. Here we report that ultrasensitive measures of circulating tumor DNA (ctDNA) and T cell expansion can be used to assess responses to immune checkpoint blockade in metastatic lung cancer patients (N=24). Patients with clinical response to therapy had a complete reduction in ctDNA levels after initiation of therapy whereas, non-responders had no significant changes or an increase in ctDNA levels. Patients with initial response followed by acquired resistance to therapy had an initial drop followed by recrudescence in ctDNA levels. Patients without a molecular response had shorter progression-free and overall survival compared to molecular responders (5.2 vs 14.5 and 8.4 vs 18.7 months, HR=5.36, 95% CI: 1.57–18.35, p=0.007 and HR=6.91, 95% CI: 1.37–34.97, p=0.02 respectively), which was detected on average 8.7 weeks earlier and was more predictive of clinical benefit than CT imaging. Expansion of T cells, measured through increases of T cell receptor (TCR) productive frequencies mirrored ctDNA reduction in response to therapy. We validated this approach in an independent cohort of early stage NSCLC patients (N=14), where the therapeutic effect was measured by pathologic assessment of residual tumor after anti-PD1 therapy. Consistent with our initial findings, early ctDNA dynamics predicted pathologic response to immune checkpoint blockade. These analyses provide an approach for rapid determination of therapeutic outcomes for patients treated with immune checkpoint inhibitors and have important implications for the development of personalized immune targeted strategies.

Keywords

ctDNA; TCR dynamics; lung cancer; immune checkpoint blockade; neoadjuvant anti-PD1 therapy

Introduction

Despite the durable clinical benefit observed with immune checkpoint inhibitors for non-small cell lung cancer (NSCLC) patients, the majority of patients are either refractory or eventually develop acquired resistance after an initial response (1). Similar to the targeted therapy paradigm, success of immuno-oncology seems to depend on choosing patient populations most likely to benefit. The plasticity of the immune system under immunotherapy has weakened single biomarker-driven approaches (2) and currently used predictive biomarkers have been unable to accurately identify the subset of patients that benefit from these therapies.

We hypothesized that non-invasive molecular analyses that evaluate tumor-derived cell free circulating tumor DNA (ctDNA) and tumor-extrinsic (TCR repertoire) parameters may be useful for rapidly determining which patients would ultimately benefit from immune checkpoint blockade. Such approaches may be of particular importance for immune targeted agents as the therapeutic responses have been challenging to evaluate using radiographic imaging due to tumor immune infiltration (3). Conventional response criteria such as the Response Evaluation Criteria in Solid Tumors (RECIST) do not consistently capture the unique patterns and timing of anti-tumor immune responses (4, 5).

The temporal relationship between detection of ctDNA and emergence of recurrent or progressive disease has been shown in patients with early stage NSCLC (6, 7) and as we show in our companion study in advanced NSCLC patients receiving targeted therapies (8). During treatment with immunotherapy, our group has shown that ctDNA may be predictive of outcome in melanoma patients treated with CTLA-4 blockade (9). ctDNA changes have been associated with therapeutic outcome during immune checkpoint blockade in NSCLC (10–12), however these analyses have been limited by the low sensitivity of the approaches, permitting analyses in approximately half of the cases analyzed. Even less is known about the dynamics of the peripheral T cell repertoire during immune checkpoint blockade in NSCLC (13) and how these changes relate to ctDNA levels and tumor response.

To overcome these issues and to allow ultrasensitive evaluation of ctDNA during therapy, we have developed targeted error-correction sequencing (TEC-Seq), a custom capture and sequencing approach that permits sensitive and specific detection of low abundance sequence alterations using next generation sequencing (14). We have also developed new methods of evaluating TCR clonal expansion in the tumor microenvironment during immune checkpoint blockade (13). Here, we use these approaches to investigate whether ctDNA and TCR dynamics are reflective of therapeutic outcome for NSCLC patients treated with immune checkpoint blockade.

Materials and Methods

Patient Characteristics

Our study group consisted of 24 metastatic NSCLC patients treated with immune checkpoint blockade as a standard of care (n=19) or in the setting of a clinical trial (n=5) between October 2014 and August 2016 at Johns Hopkins Sidney Kimmel Cancer Center. In parallel, we evaluated 14 patients with stage I-IIIA surgically resectable NSCLC that received anti-PD1 therapy in the setting of a neoadjuvant nivolumab clinical trial (15). The studies were conducted in accordance with the Declaration of Helsinki, were approved by the Institutional Review Board (IRB) and patients provided written informed consent for sample acquisition for research purposes. Clinical characteristics for all patients are summarized in Supplementary Table S1.

Treatment and assessment of therapeutic response

Therapeutic responses were evaluated by the Response Evaluation criteria in Solid Tumors (RECIST) version 1.1 (16). Baseline disease burden was determined by the sum of the longest diameters of target lesions as determined by RECIST 1.1 criteria. After baseline imaging, radiographic evaluation was performed at 5–10 week intervals or as clinically indicated for the metastatic cohort and 7 days prior to surgery for the early stage cohort. The timing of radiologic assessments typically followed the early timepoints of blood sample collection. Although this approach may be subject to lead-time bias, we sought to mirror the imaging schedule used in clinical practice. Furthermore, in contrast to chemotherapy or targeted therapy, where therapeutic response may be accurately evaluated by imaging early after treatment initiation, the unique nature and timing of response to immune checkpoint blockade mandates response assessments at later timepoints including confirmation of the

radiologic response. Of the 19 metastatic NSCLC patients with detectable ctDNA, 1 achieved complete response (CGLU111), 3 patients achieved partial response (CGLU135, CGLU337 and CGLU347) and 12 achieved SD (CGLU115, CGLU117, CGLU159, CGLU160, CGLU162, CGLU168, CGLU203, CGLU211, CGLU212, CGLU340, CGLU351 and CGLU357) as best overall response. Three patients (CGLU121, CGLU243 and CGLU348) experienced disease progression. Of the 3 patients with partial response, 2 eventually developed molecular resistance. In the neoadjuvant cohort, a repeat chest CT ≤7 days prior to surgery revealed stable disease for all patients with detectable ctDNA at baseline.

PFS and OS were defined as the time elapsed between the date of treatment initiation and the date of disease progression or death from disease, or the date of death, respectively (Supplementary Table S1). For the early stage cases with detectable ctDNA, two patients demonstrated a major pathologic response (pMPR defined as ≥90% decrease in tumor burden; CGLU206 and CGLU249), 3 patients had a partial pathologic response (at least 30% decrease in the tumor burden; CGLU205, CCGLU219 and CGLU221) and 2 patients had a pathologic nonresponse (CGLU222 and CGLU225).

Blood sample collection

For all patients, at least 2 serial blood samples (range 2–8) were collected over the course of treatment for isolation of plasma and extraction of cell-free DNA for genomic analyses. We analyzed a total of 105 serial plasma samples that were obtained prior to anti-PD1, at 4–8 weeks and additional time points during therapy for all metastatic NSCLC patients except for CGLU135 and CGLU161. For these two patients, blood from early timepoints was not available and blood samples from the time of radiographic response and the time of acquired resistance were analyzed. A detailed description of the time points analyzed is shown in Supplementary Tables S2 and S3. Baseline tumors were analyzed by whole exome sequencing or targeted next generation sequencing for patients in the metastatic cohort, with the exception of CGLU168 for which a tumor specimen from the time of resistance to immune checkpoint blockade was used. For the early stage cohort tumor samples prior to therapy initiation or at the time of resection in the cases where baseline tumor was not available, were analyzed by whole exome sequencing (15).

Sample preparation and next-generation sequencing of cfDNA

Whole blood was collected in K2 EDTA tubes; plasma and cellular components were separated by centrifugation at 800g for 10 minutes at 4°C. Plasma was centrifuged a second time at 18,000g at room temperature to remove any remaining cellular debris and stored at −80°C until the time of DNA extraction. DNA was isolated from plasma using the Qiagen Circulating Nucleic Acids Kit (Qiagen GmbH, Hilden DE). TEC-Seq next-generation sequencing cell-free DNA libraries were prepared from 12 to 125 ng of cfDNA. Genomic libraries were prepared as previously described and targeted capture was performed using the Agilent SureSelect reagents and a custom set of hybridization probes targeting 58 genes, described in Supplementary Table S4 (14). TEC-Seq libraries were sequenced using 100 bp paired end runs on the Illumina HiSeq 2500 (Illumina, San Diego, CA). The analytical

performance and validation including sensitivity and specificity and limits of detection of our ctDNA platform have been recently reported (14).

Primary processing of cfDNA next-generation sequencing data and identification of putative somatic mutations

Primary processing of next-generation sequence data for cfDNA samples was performed as previously described (14) using Illumina CASAVA software (v1.8), including demultiplexing and masking of dual index adapter sequences. Sequence reads were aligned against the human reference genome (hg19) using Novoalign with additional realignment of select regions using the Needleman-Wunsch method (17). Next, candidate somatic mutations, consisting of point mutations, small insertions, and deletions were identified using VariantDx (17) across the targeted regions of interest. VariantDx examined sequence alignments of cfDNA plasma samples while applying filters to exclude alignment and sequencing artifacts as previously described (14). Specifically, an alignment filter was applied to exclude quality failed reads, unpaired reads, and poorly mapped reads in the plasma. A base quality filter was applied to limit inclusion of bases with reported Phred quality score > 30. Criteria for calling alterations in cfDNA have been previously described (14). TEC-Seq characteristics are shown in Supplementary Table S5.

Definition of tumor-derived cfDNA

Genomic alterations in ctDNA were cross-referenced against each patient's tumor-specific genomic alterations to identify bona fide tumor specific ctDNA variants. Variants identified in ctDNA as previously described (14) as well as in the matching tumor with a MAF of ≥2% were considered tumor-specific. We focused on somatic variants that were identified both in the tumor sample as well as in ctDNA for each patient to exclude variants related to clonal hematopoiesis (Supplementary Table S6). Our dataset is deposited in the database of Genotypes and Phenotypes (dbGaP; study ID 32485).

Clonality estimates of cfDNA variants

To assess the cellular prevalence of plasma mutations in their corresponding tumors, tumor samples of each case were analyzed as follows. The density of reads mapping to target and off-target regions in tumor whole exome sequence data was corrected for GC content, target size, and sequence complexity and compared to a reference panel of normal samples to establish log copy ratio values as a measure of relative copy number across the genome (18). Bin-level copy ratio values were segmented using circular binary segmentation (19). Segment copy ratio values and minor allele frequency of germline heterozygous SNPs overlapping the segments were analyzed to determine the purity and ploidy of the sample, and allele-specific copy number for segments using an in-house pipeline. Next, we used SCHISM (20) to determine the cellular prevalence of mutations based on the observed variant allele frequency, estimated copy number, and sample purity by following an approach similar to that previously described (13). This approach to clonality assessment was not feasible for mutations in four cases (CGLU168, CGLU206, CGLU219 and CGLU249) where purity and ploidy could not be determined due to low tumor content. Mutation cellularity analysis is summarized in Supplementary Table S7.

T cell receptor sequencing and differential expansion analyses

TCR clones were evaluated in pre-treatment tumor tissue (with the exception of CGLU117, where tumor tissue from the time of resistance was also analyzed), and 40 serial peripheral blood lymphocytes (PBLs) by next generation sequencing in the metastatic NSCLC cohort (Supplementary Table S8). DNA from pre-treatment tumor samples and PBLs was isolated by using the Qiagen DNA FFPE and Qiagen DNA blood mini kit respectively (Qiagen, CA). TCR-β CDR3 regions were amplified using the survey (tumor) or deep (PBLs) ImmunoSeq assay in a multiplex PCR method using 45 forward primers specific to TCR Vβ gene segments and 13 reverse primers specific to TCR Jβ gene segments (Adaptive Biotechnologies) (21, 22). Productive TCR sequences were further analyzed. TCR sequencing data from TILs was used to identify tumor-specific TCR clonotypes in the peripheral blood. Peripheral TCR clones achieving a frequency of at least 0.005% were evaluated for differential abundance between baseline and the time of radiographic response using Fisher's exact test with False Discovery Rate (FDR) p-value correction (corrected $P \leq 0.05$). Those differentially abundant clones also found in the tumor were further selected to determine their frequencies in peripheral blood prior to treatment, at the time of response and upon emergence of resistance (Supplementary Tables S9–S18). We calculated the average productive frequency of differentially abundant clones and used it as a metric of TCR dynamics during therapy. To cluster significantly expanded intratumoral TCR-β CDR3s based on potential recognition specificity, we employed the GLIPH method (Grouping of Lymphocyte Interactions by Paratope Hotspots) (23).

CDR3 and VJ gene usage analyses

Subsequent to initial filtering, we further reduced noise by eliminating clones that did not have frequencies beyond a mean rate of 5 counts. Thus, when 2 points were examined (baseline and time of radiologic response), the total sum of counts were greater or equal to 10. Using these data, we examined the usage of CDR3b Variable (V) and Joining (J) regions, and their overall clonal composition by known significant clones at the 2 time points.

Multiplex Cytokine Immunoassay

We employed a multiplex bead-based immunoassay on the Luminex platform that examines cytokines involved in T cell activation, expansion, differentiation and long-term proliferation (IFN-gamma, IL-1, IL-2), Th1 immune response (IL-12), acquisition of the Th2 phenotype (IL-4) as well as immunosuppressive cytokines important for regulatory T cells (IL-10) in four patients of the early stage cohort where additional serum was available. Differences in concentration of cytokines were evaluated between baseline and on treatment (week 2–6) samples.

Statistical analyses

ctDNA values were dichotomized as detectable and undetectable. Characteristics for each group were compared using chi-square or Fischer's exact test for categorical variables. Pearson correlation coefficient (R) was used to assess correlations between continuous variables. Differences between molecular responders and non-responders were assessed by the Mann-Whitney test. Tumors were classified based on their non-synonymous sequence

alteration load in high and low mutators as previously described (24). The median point estimate and 95% CI for PFS and OS were estimated by the Kaplan–Meier method. Survival curves were compared by using the log-rank test. Univariate Cox proportional hazards regression analysis was used to determine the impact of ctDNA molecular response on progression-free and overall survival. All p values were based on two-sided testing and differences were considered significant at $p < 0.05$. Statistical analyses were done using the SPSS software program (version 25.0.0 for Windows, IBM, Armonk, NY).

Results

Overall approach and patient characteristics

We analyzed 105 serial blood samples from 38 NSCLC patients, including 24 patients with metastatic NSCLC during immune checkpoint blockade and 14 patients with stage I-IIIA surgically resectable NSCLC that received anti-PD1 therapy as part of a clinical trial of neoadjuvant nivolumab (15) (Table 1 and Supplementary Table S1). The median duration of follow-up was12.7 months (range 3.0–37.8 months) and 16 months (range 2–30 months) for the metastatic and early stage patients respectively and median duration of treatment was 7 months (range 1–20 months) for the metastatic cohort. We evaluated response to immune checkpoint blockade using standard computed tomographic (CT) imaging and changes in tumor burden were assessed by RECIST 1.1. Blood samples for the metastatic NSCLC patients were prospectively collected prior to therapy, at an early time point between 4 and 8 weeks from treatment initiation and at additional serial time points during therapy until the time of disease progression (Supplementary Tables S2 and S3). For the early stage NSCLC patients treated with anti-PD1 therapy in the neoadjuvant setting, blood samples were collected prior to immunotherapy, at 2 weeks, immediately prior to resection and post-resection (Supplementary Table S2). ctDNA was measured using the TEC-Seq approach (14) and the TCR repertoire was studied longitudinally by means of TCR sequencing (Figure 1). Given the possibility of hematopoietic alterations which may be detected in the plasma (14), especially in heavily treated patients, we focused only on tumor-specific sequence alterations in cell-free DNA. Clinical characteristics, outcome and liquid biopsy analyses are summarized in Table 1.

ctDNA dynamics and tumor response

In the metastatic NSCLC cohort, ctDNA was detected in 19 of 24 patients either at baseline (n=14) or at other time points when baseline samples were not available (n=5), with a median mutant allele fraction of 1.87% (range 0.09%−34.7%). In the early stage cohort, ctDNA was detected at baseline in 7 of 14 patients, with a median allele fraction of 0.34% (range 0.15%−2.19%). For patients with detectable ctDNA, an average of 1 tumor-specific alterations were detected (median 1, range 1–4) affecting one or more of 12 driver genes, including those commonly altered in lung cancer (Supplementary Tables S4–S6). The vast majority of tumor-specific variants were clonal in the corresponding tumor samples (Supplementary Table S7).

We observed three patterns of molecular response in ctDNA for patients treated with immune checkpoint inhibitors. Among the patients with a molecular response (n=9),

individuals had a dramatic reduction in ctDNA to undetectable levels on average at 9 weeks from treatment initiation (Figure 2A–E and Supplementary Figure S1). As an example, for patient CGLU111 with a sustained clinical response, ctDNA-based molecular analyses showed a complete molecular response at week 4, more than 5 weeks prior to a radiologic partial response and 26 weeks earlier than complete radiologic response determined by RECIST 1.1 (Figure 2). In contrast, for patients with a pattern of molecular resistance (n=10), ctDNA levels had limited fluctuations or displayed a rise 3–16 weeks after therapeutic initiation. As a representative patient, ctDNA levels in CGLU121 continued to rise from the time of initiation of immune checkpoint blockade, consistent with radiographic disease progression (Figure 3A–E). All patients with ctDNA features of primary molecular resistance had radiologic disease progression that followed molecular resistance by 5.5 weeks (Supplementary Figure S2).

The third observed pattern, seen in five of the molecular responders, was one consistent with molecular acquired resistance, where ctDNA dynamics reflected clonal evolution under selective pressure of anti-PD1 therapy and emergence of immune escape. In such cases, tumor-specific variants were undetectable at the time of response followed by increase in mutant allele fraction at the time of acquired resistance (Supplementary Figure S1). Emergence of molecular resistance preceded disease progression on imaging by an average of 10.8 weeks. Overall, ctDNA-based molecular responses were detected on average 8.7 weeks earlier than conventional RECIST1.1 response assessment (6.7 vs 15.4 weeks, p=0.004, Supplementary Figure S3).

Early ctDNA clearance was a significant prognostic factor for progression-free (PFS) and overall survival (OS). Patients with a reduction of ctDNA to undetectable levels demonstrated a significantly longer PFS and OS compared to patients with no evidence of ctDNA elimination (log rank p=0.001 and p=0.008 respectively, Figure 4A and B and Supplementary Figure S4). The duration of the molecular responses tightly correlated with progression-free and overall survival (Supplementary Figure S5).

Radiographic imaging at the time of first assessment was a worse predictor of outcome to anti-PD1 therapy compared to ctDNA molecular response for these patients (Figure 4A–B and Supplementary Figure S6). Patients with radiographically stable disease (n=12) had differential responses to immune checkpoint blockade that were consistent with their molecular response pattern (Supplementary Figure S7). More specifically, five patients with stable disease by imaging showed a clear molecular response pattern, with ctDNA elimination between week 4 and 13 from immune checkpoint blockade initiation (Supplementary Figure S1). All five patients derived clinical benefit from PD-1 blockade (PFS and OS ranging from 7.3–13.6 and 12–21.3 months, respectively, Supplementary Figure S7), suggesting that imaging failed to detect the magnitude of therapeutic response.

Interestingly, ctDNA molecular responses more accurately predicted PFS and OS compared to tumor mutation burden in our cohort (TMB; Supplementary Figure S8). When TMB and ctDNA were combined the ctDNA-based molecular responders clustered together independent of the TMB for both PFS and OS (Figure 4C–D). Given that clonal mutation burden may be a more accurate predictor of response to immune checkpoint blockade, we

performed survival analyses incorporating clonal TMB and we again found that ctDNA dynamics predict survival independent of clonal TMB status (Supplementary Figure S9).

Molecular responses predict pathologic response to immune checkpoint blockade

Given the challenges with radiologic response assessments to immune checkpoint blockade, we sought to validate our observations in a NSCLC cohort where the therapeutic effect was measured at a pathologic level instead of using conventional imaging. We analyzed serial plasma samples from a recently reported clinical trial of neoadjuvant nivolumab for early stage operable NSCLC (15). For these patients the therapeutic effect was rigorously measured by pathologic assessment of residual tumor after two doses of anti-PD1 therapy (15, 25). Similar to our initial analyses, we observed that all tumors with a major or partial pathologic response to anti-PD1 therapy demonstrated a molecular response pattern of elimination of tumor-specific mutations in the circulation (Figure 5A and Supplementary Figure S10). In contrast, tumors without a pathologic response demonstrated a molecular resistance pattern at the time of resection of the primary tumor (Figure 5B and Supplementary Figure S10).

Peripheral TCR landscape and therapeutic outcome

We investigated how immune checkpoint blockade affects the peripheral TCR repertoire and whether there are TCR clonotype dynamic changes reflective of a systemic anti-tumor immune response. We focused our analyses on TCR clones found in the tumor microenvironment using TCR sequencing and investigated their dynamics in the peripheral blood, identifying those with a statistically significant differential abundance from baseline. Twelve of the 24 metastatic NSCLC patients had available samples from both tumor infiltrating lymphocytes as well as peripheral blood lymphocytes for analysis (Supplementary Table S3 and S8), including five that had previously undergone TCR sequencing (13) but had not been analyzed using this approach.

Similar to ctDNA analyses, we observed distinct patterns in TCR clonotype dynamics among the analyzed patients. For patients with clinical responses to immune checkpoint blockade, a statistically significant oligoclonal expansion of pre-existing intra-tumoral T cell clones was observed in peripheral blood at the time of radiologic response to PD1 blockade (CGLU111, CGLU117, CGLU127 and CGLU212) (Figure 2, Supplementary Figure S11, and Supplementary Tables S9–12). For patients that developed acquired resistance, productive frequencies of intratumoral clones significantly decreased in peripheral blood at the time of acquired resistance (CGLU117, CGLU127, CGLU135 and CGLU161) (Supplementary Figure S11 and Supplementary Tables S10, S11, S13, S14), with a timing that was similar to ctDNA analyses for most cases.

In contrast, for patients CGLU121 and CGLU115 that had primary resistance to immunotherapy, we did not identify any differentially abundant TCR clones among serial peripheral blood samples (Figure 3 and Supplementary Figure S12). These patients progressed radiographically within 5–13 weeks from initiation of therapy and, in line with the clinical course, there was no evidence of TCR clonal expansion among the intratumoral TCR repertoire. A transient oligoclonal TCR expansion was observed for non-responding

patient CGLU159 at week 11, however productive frequencies of differentially abundant clones quickly decreased to baseline levels at week 16, which coincided with disease progression (Supplementary Figure S12, Supplementary Table S15). Patients CGLU162, CGLU203 and CGLU243 had 1–26 intratumoral TCR clones with differential abundance at the time of best radiographic response compared to baseline but were classified as ctDNA molecular non-responders (Supplementary Figure S12 and Supplementary Tables S16–18). Patients CGLU203 and CGLU243 had unfavorable outcome to anti-PD1 therapy, suggesting that for these patients, ctDNA kinetics may more accurately predict therapeutic outcome.

We did not identify any shared TCR clones among the differentially expanded ones for all patients analyzed, consistent with the notion that the mutation-associated neoantigen repertoires are largely private. We evaluated putative shared CDR3 motifs among significantly expanded TCR clones employing the grouping of lymphocyte interactions by paratope hotspots algorithm (23). Interestingly, TCR clones CSARVGVGNTIYF and CSARSGVGNTIYF, that were differentially abundant at the time of response to immune checkpoint blockade for patient CGLU127 and CGLU135, respectively, clustered together, suggesting a common specificity to a tumor- or mutation-associated antigen. We subsequently investigated potential differential sequence features focusing on Variable (V) and Joining (J) gene usage and CDR3 lengths among different timepoints for each patient. Usage of specific V and J gene segments increased at the time of response compared to baseline for a patient with sustained response (CGLU111) in contrast to a representative patient with primary resistance (CGLU121, Supplementary Figure S13). Our findings on differential V gene usage may suggest clonotypic amplifications of specific immune subsets (CD8+ vs. CD4+) during immune checkpoint blockade (26).

Discussion

The unique nature of responses to immune checkpoint blockade (27, 28) and known limitations of conventional radiologic response assessments (3) highlight the need for development of biomarker-driven approaches to interpret therapeutic responses. Success of immunotherapy approaches depends on choosing patient populations most likely to benefit. There is therefore an urgent clinical need for molecular assays of response and resistance to immune targeted agents. To this end, we analyzed ctDNA and TCR clonal dynamics during immune checkpoint blockade in NSCLC and assessed the value of longitudinal monitoring of liquid biopsies as a surrogate for response to therapy. Our findings indicate that ctDNA dynamics after treatment initiation may allow patients with primary resistance to immune checkpoint blockade to be rapidly identified and redirected to receive alterative options.

Non-invasive detection and monitoring of acquired resistance to EGFR targeted therapy has been evaluated by serial sampling of ctDNA (29, 30) and as we have shown in a complementary study, changes in ctDNA levels may predict response to targeted therapy in NSCLC (8). Longitudinal assessment of ctDNA in metastatic melanoma patients receiving anti-PD1 therapy has been demonstrated to be an accurate predictor of tumor response and therapeutic outcome (31) and early ctDNA clearance may correlate with durable clinical benefit to PD-1 blockade (10, 12). ctDNA dynamics may be also informative in differentiating pseudoprogression from disease progression during immunotherapy (32).

However, these approaches have been limited by low sensitivity and specificity of ctDNA methods, with many patients lacking detectable alterations and potential admixture between tumor alterations and those involved in clonal hematopoiesis (33, 34).

Moreover, interpretation of ctDNA analyses without knowledge of tumor-specific somatic alterations may be difficult in the setting of heavily pre-treated patient populations such as late-stage lung cancer patients, given the mutagenic effects of systemic chemotherapy and ionizing radiation on cells of the myeloid lineage (35). To address the possible presence of alterations in cfDNA from clonal non-malignant hematopoietic cells, we have focused our analyses of variants in ctDNA that were also identified through next generation sequencing of the matched tumor, allowing distinction of tumor-specific from blood cell proliferation variants.

Clonal expansion of intra-tumoral T cells may predict therapeutic outcome for immune checkpoint blockade (36), however little is known about the significance of peripheral expansion of TCR clones found in the tumor microenvironment during therapy. Expansion of peripheral CD8+ T cell populations has been shown to precede immune-related adverse events in patients treated with ipilimumab (37). We investigated whether the NSCLC patients in our cohort developed immune-related adverse events at the time of TCR clonal expansion and did not identify a definitive pattern with the exception of patient CGLU243, where pneumonitis emerged shortly after treatment initiation. While there were cases for which TCR expansion preceded the development of a grade 2–4 immune-related adverse event (CGLU161, CGLU117), such events were also noted significantly later from the time of TCR expansion (CGLU111, CGLU135). These observations highlight the challenges with interpretation of the evolving peripheral TCR repertoire. Assessing the quality of the immune response in conjunction with clonotypic amplifications may provide additional information on the evolving TCR repertoire; to this end, we looked at differences in cytokine levels in selected early stage patients with available serum at baseline and 2–6 weeks during anti-PD1 therapy. We did not identify any significant changes in cytokine levels in peripheral blood between baseline and week 2–6 on anti-PD1 therapy however these analyses were limited by small number of cases tested (Supplementary Figure S14).

In summary, we have developed dynamic assays that capture the tumor-immune system equilibrium and assess immune editing of neoantigens during immunotherapy. We have shown that these approaches have advantages compared conventional radiologic response assessment and static molecular analyses such as baseline TMB. We believe that these methods are especially suited for the interpretation of unique responses seen with immune targeted agents that are not adequately captured by traditional response criteria. In addition to more accurately predicting long term response to immunotherapy, we were able to predict therapeutic outcome on average 8.7 weeks earlier than radiographic imaging. However, our work is limited by the small sample size, cohort heterogeneity and retrospective nature of the analyses. Validation of these findings may lead to early therapeutic decisions to ensure that an ineffective treatment is discontinued as well as allow response adaptive combination and sequencing of subsequent therapies. Additional work will be needed to address the frequency of serial monitoring and feasibility of interpreting ctDNA dynamics without prior knowledge of tumor mutations. Prospective studies will be needed to assess whether

switching therapy based on ctDNA dynamics prior to radiologic progression will improve outcome and ultimately whether a liquid biopsy approach can replace conventional imaging as a gold standard for early response assessment to immune checkpoint blockade.

Supplementary Material

Refer to Web version on PubMed Central for supplementary material.

Acknowledgements

This work was supported in part by US National Institutes of Health grants CA121113 (V.Velculescu, V. Anagnostou), CA006973 (D. Pardoll, V. Velculescu), CA180950 (V. Velculescu), the Commonwealth Foundation (V. Velculescu), the Bloomberg-Kimmel Institute for Cancer Immunotherapy (V. Anagnostou, P. Forde, J. Brahmer, D. Pardoll, V. Velculescu), the Dr. Miriam and Sheldon G. Adelson Medical Research Foundation (V. Velculescu), the Eastern Cooperative Oncology Group-American College of Radiology Imaging Network (V. Anagnostou), MacMillan Foundation (V. Anagnostou), the V Foundation (V. Anagnostou, V. Velculescu), the ICTR-ATIP UL1TR001079 (V. Anagnostou), the Pardee Foundation (V. Anagnostou), Swim Across America (V. Anagnostou), the William R. Brody Faculty Scholarship (R. Karchin), the SU2C-ACS Lung Cancer Dream Team (P. Forde and E. Gabrielson), PRIME Oncology (J. Naidoo), the MSK Cancer Center Support Grant/Core Grant (P30 CA008747), the SU2C DCS International Translational Cancer Research Dream Team Grant (SU2C-AACR-DT1415; V. Velculescu), the SU2C-LUNGevity-American Lung Association Lung Cancer Interception Dream Team (J. Brahmer, V. Velculescu), the Allegheny Health Network - Johns Hopkins Research Fund (V. Anagnostou, V. Velculescu), the LUNGevity Foundation (V. Anagnostou and P. Forde), the Mark Foundation (A. Leal, V. Velculescu), and Bristol Meyers Squibb (P. Forde). Stand Up To Cancer is a program of the Entertainment Industry Foundation administered by the American Association for Cancer Research. This publication was made possible in part by the Johns Hopkins Institute for Clinical and Translational Research (ICTR), which is funded in part by Grant Number UL1TR001079 from the National Center for Advancing Translational Sciences (NCATS) a component of the National Institutes of Health (NIH), and NIH Roadmap for Medical Research. Its contents are solely the responsibility of the authors and do not necessarily represent the official view of the Johns Hopkins ICTR, NCATS or NIH.

We thank Dr. Suzanne Topalian and members of our laboratories for helpful discussions and critical review of the manuscript.

Disclosure of potential conflicts of interest

P.M.F. receives research funding for clinical trials from Bristol-Myers Squibb, AstraZeneca/MedImmune, Kyowa, Corvus and Novartis and is a consultant/advisory board member for Abbvie, AstraZeneca, Bristol-Meyers Squibb, Boehringer Ingelheim, Celgene, EMD Serono, Inivata, Lilly, Merck, and Novartis. J.W. is a consultant for Personal Genome Diagnostics. J.N. receives research funding from Merck, AstraZeneca/MedImmune, Kyowa and Calithera and is a consultant/advisory board member of Bristol-Myers Squibb, AstraZeneca/MedImmune and Takeda. C.L.H is a consultant/advisory board member for AbbVie, Bristol-Myers Squibb and Genentech, receives research funding from Merrimack, GlaxoSmithKline, AbbVie, Bristol-Myers Squibb, and GlaxoSmithKline. J.S. owns Merck, Pfizer, Thermo Fisher Scientific and Chemed Corporation stock. J.T. is an advisory board member of Bristol-Meyers Squib, Merck, Astra Zeneca and Amgen and receives research funding from Bristol-Meyers Squib. B.L is a consultant/advisory board member of AstraZeneca, Celgene, Genentech Rouche, Eli Lilly, and Takeda and receives research funding from Celgene and Boehringer Ingleheim. J.R.B. receives research grants from Bristol-Myers Squibb, AstraZeneca/MedImmune and Merck and is a consultant/advisory board member for Bristol-Myers Squibb, AstraZeneca/MedImmune and Merck. C.Z. receives research grants from Janssen. M.V.B. is a paid consultant for Cepheid Inc. J.I. owns LumaCyte, LLC. Stock. M.D.H. receives research funding from Bristol-Myers Squibb; is a paid consultant to Merck, Bristol-Myers Squibb, AztraZeneca, Genentech/Roche, Janssen, Nektar, Syndax, Mirati, and Shattuck Labs; and a patent has been filed by MSK related to the use of tumor mutation burden to predict response to immunotherapy (PCT/US2015/062208). J.E.C. is a paid consultant to Merck, Bristol-Myers Squibb, AstraZeneca, Genetech/Roche and is the named investigator on institutional research grants from Bristol-Myers Squibb, Genentech, and AstraZeneca. D.M.P. receives research support from Bristol-Myers Squibb, Compugen and Potenza Therapeutics and is a consultant for Aduro Biotech, Amgen, AstraZeneca/Medimmune, Bayer, Compugen, DNAtrix, Five Prime, GlaxoSmithKline, ImmuneXcite, Jounce Therapeutics, Neximmune, Pfizer, Rock Springs Capital, Sanofi and Vesuvius/Tizona. V.E.V. is a founder of, holds equity in, and is a member of the Board of Directors of Personal Genome Diagnostics (PGDx). Under a license agreement between PGDx and the Johns Hopkins University, V.E.V. is entitled to a share of royalty received by the University on sales of services or products by PGDx. V.E.V. is a member of the Scientific Advisory Board of Ignyta. The terms of these arrangements have been reviewed and approved by the Johns Hopkins University in accordance with its conflict of interest policies.

References

1. Horn L, Spigel DR, Vokes EE, Holgado E, Ready N, Steins M, et al. Nivolumab Versus Docetaxel in Previously Treated Patients With Advanced Non-Small-Cell Lung Cancer: Two-Year Outcomes From Two Randomized, Open-Label, Phase III Trials (CheckMate 017 and CheckMate 057). Journal of clinical oncology: official journal of the American Society of Clinical Oncology. 2017;35(35):3924–33. doi: 10.1200/JCO.2017.74.3062. [PubMed: 29023213]
2. Sharma P, Allison JP. The future of immune checkpoint therapy. Science. 2015;348(6230):56–61. doi: 10.1126/science.aaa8172. [PubMed: 25838373]
3. Anagnostou V, Yarchoan M, Hansen AR, Wang H, Verde F, Sharon E, et al. Immuno-oncology Trial Endpoints: Capturing Clinically Meaningful Activity. Clinical cancer research : an official journal of the American Association for Cancer Research. 2017;23(17):4959–69. doi: 10.1158/1078-0432.CCR-16-3065.
4. Hodi FS, Hwu WJ, Kefford R, Weber JS, Daud A, Hamid O, et al. Evaluation of Immune-Related Response Criteria and RECIST v1.1 in Patients With Advanced Melanoma Treated With Pembrolizumab. J Clin Oncol. 2016;34(13):1510–7. doi: 10.1200/JCO.2015.64.0391. [PubMed: 26951310]
5. Bohnsack O, Hoos A, Ludajic K. Adaptation of the immune related response criteria: irRECIST. Ann Oncol. 2014;Supplement 4:iv361–iv72.
6. Abbosh C, Birkbak NJ, Wilson GA, Jamal-Hanjani M, Constantin T, Salari R, et al. Phylogenetic ctDNA analysis depicts early-stage lung cancer evolution. Nature. 2017;545(7655):446–51. doi: 10.1038/nature22364. [PubMed: 28445469]
7. Jamal-Hanjani M, Wilson GA, McGranahan N, Birkbak NJ, Watkins TBK, Veeriah S, et al. Tracking the Evolution of Non-Small-Cell Lung Cancer. The New England journal of medicine. 2017;376(22):2109–21. doi: 10.1056/NEJMoa1616288. [PubMed: 28445112]
8. Phallen J, Leal A, Woodward B, Forde PM, Naidoo J, Marrone K, et al. Early Noninvasive Detection of Response to Targeted Therapy in Non-Small Cell Lung Cancer. Submitted. 2018.
9. Lipson EJ, Velculescu VE, Pritchard TS, Sausen M, Pardoll DM, Topalian SL, et al. Circulating tumor DNA analysis as a real-time method for monitoring tumor burden in melanoma patients undergoing treatment with immune checkpoint blockade. J Immunother Cancer. 2014;2(1):42. doi: 10.1186/s40425-014-0042-0. [PubMed: 25516806]
10. Cabel L, Riva F, Servois V, Livartowski A, Daniel C, Rampanou A, et al. Circulating tumor DNA changes for early monitoring of anti-PD1 immunotherapy: a proof-of-concept study. Annals of oncology : official journal of the European Society for Medical Oncology / ESMO. 2017;28(8): 1996–2001. doi: 10.1093/annonc/mdx212.
11. Iijima Y, Hirotsu Y, Amemiya K, Ooka Y, Mochizuki H, Oyama T, et al. Very early response of circulating tumour-derived DNA in plasma predicts efficacy of nivolumab treatment in patients with non-small cell lung cancer. Eur J Cancer. 2017;86:349–57. doi: 10.1016/j.ejca.2017.09.004. [PubMed: 29078173]
12. Goldberg SB, Narayan A, Kole AJ, Decker RH, Teysir J, Carriero NJ, et al. Early Assessment of Lung Cancer Immunotherapy Response via Circulating Tumor DNA. Clinical cancer research : an official journal of the American Association for Cancer Research. 2018. doi: 10.1158/1078-0432.CCR-17-1341.
13. Anagnostou V, Smith KN, Forde PM, Niknafs N, Bhattacharya R, White J, et al. Evolution of Neoantigen Landscape during Immune Checkpoint Blockade in Non-Small Cell Lung Cancer. Cancer discovery. 2017;7(3):264–76. doi: 10.1158/2159-8290.CD-16-0828. [PubMed: 28031159]
14. Phallen J, Sausen M, Adleff V, Leal A, Hruban C, White J, et al. Direct detection of early-stage cancers using circulating tumor DNA. Science translational medicine. 2017;9(403). doi: 10.1126/scitranslmed.aan2415.
15. Forde PM, Chaft JE, Smith KN, Anagnostou V, Cottrell TR, Hellmann MD, et al. Neoadjuvant PD-1 Blockade in Resectable Lung Cancer. The New England journal of medicine. 2018. doi: 10.1056/NEJMoa1716078.

16. Eisenhauer EA, Therasse P, Bogaerts J, Schwartz LH, Sargent D, Ford R, et al. New response evaluation criteria in solid tumours: revised RECIST guideline (version 1.1). European journal of cancer. 2009;45(2):228–47. doi: 10.1016/j.ejca.2008.10.026. [PubMed: 19097774]

17. Jones S, Anagnostou V, Lytle K, Parpart-Li S, Nesselbush M, Riley DR, et al. Personalized genomic analyses for cancer mutation discovery and interpretation. Science translational medicine. 2015;7(283):283ra53. doi: 10.1126/scitranslmed.aaa7161.

18. Talevich E, Shain AH, Botton T, Bastian BC. CNVkit: Genome-Wide Copy Number Detection and Visualization from Targeted DNA Sequencing. PLoS Comput Biol. 2016;12(4):e1004873. doi: 10.1371/journal.pcbi.1004873. [PubMed: 27100738]

19. Olshen AB, Venkatraman ES, Lucito R, Wigler M. Circular binary segmentation for the analysis of array-based DNA copy number data. Biostatistics. 2004;5(4):557–72. doi: 10.1093/biostatistics/kxh008. [PubMed: 15475419]

20. Niknafs N, Beleva-Guthrie V, Naiman DQ, Karchin R. SubClonal Hierarchy Inference from Somatic Mutations: Automatic Reconstruction of Cancer Evolutionary Trees from Multi-region Next Generation Sequencing. PLoS Comput Biol. 2015;11(10):e1004416. doi: 10.1371/journal.pcbi.1004416. [PubMed: 26436540]

21. Carlson CS, Emerson RO, Sherwood AM, Desmarais C, Chung MW, Parsons JM, et al. Using synthetic templates to design an unbiased multiplex PCR assay. Nature communications. 2013;4:2680. doi: 10.1038/ncomms3680.

22. Robins HS, Campregher PV, Srivastava SK, Wacher A, Turtle CJ, Kahsai O, et al. Comprehensive assessment of T-cell receptor beta-chain diversity in alphabeta T cells. Blood. 2009;114(19):4099–107. doi: 10.1182/blood-2009-04-217604. [PubMed: 19706884]

23. Glanville J, Huang H, Nau A, Hatton O, Wagar LE, Rubelt F, et al. Identifying specificity groups in the T cell receptor repertoire. Nature. 2017;547(7661):94–8. doi: 10.1038/nature22976. [PubMed: 28636589]

24. Wood DE, White JR, Georgiadis A, Van Emburgh B, Parpart-Li S, Mitchell J, et al. A machine learning approach for somatic mutation discovery. Science translational medicine. 2018;10(457). doi: 10.1126/scitranslmed.aar7939.

25. Cottrell TR, Thompson ED, Forde PM, Stein JE, Duffield AS, Anagnostou V, et al. Pathologic features of response to neoadjuvant anti-PD-1 in resected non-small-cell lung carcinoma: a proposal for quantitative immune-related pathologic response criteria (irPRC). Annals of oncology : official journal of the European Society for Medical Oncology / ESMO. 2018;29(8):1853–60. doi: 10.1093/annonc/mdy218.

26. Riaz N, Havel JJ, Makarov V, Desrichard A, Urba WJ, Sims JS, et al. Tumor and Microenvironment Evolution during Immunotherapy with Nivolumab. Cell. 2017;171(4):934–49 e15. doi: 10.1016/j.cell.2017.09.028. [PubMed: 29033130]

27. Topalian SL, Drake CG, Pardoll DM. Targeting the PD-1/B7-H1(PD-L1) pathway to activate anti-tumor immunity. Current opinion in immunology. 2012;24(2):207–12. doi: 10.1016/j.coi.2011.12.009. [PubMed: 22236695]

28. Pardoll DM. The blockade of immune checkpoints in cancer immunotherapy. Nature reviews. 2012;12(4):252–64. doi: 10.1038/nrc3239.

29. Murtaza M, Dawson SJ, Tsui DW, Gale D, Forshew T, Piskorz AM, et al. Non-invasive analysis of acquired resistance to cancer therapy by sequencing of plasma DNA. Nature. 2013;497(7447):108–12. doi: 10.1038/nature12065. [PubMed: 23563269]

30. Oxnard GR, Paweletz CP, Kuang Y, Mach SL, O'Connell A, Messineo MM, et al. Noninvasive detection of response and resistance in EGFR-mutant lung cancer using quantitative next-generation genotyping of cell-free plasma DNA. Clinical cancer research : an official journal of the American Association for Cancer Research. 2014;20(6):1698–705. doi: 10.1158/1078-0432.CCR-13-2482.

31. Lee JH, Long GV, Boyd S, Lo S, Menzies AM, Tembe V, et al. Circulating tumour DNA predicts response to anti-PD1 antibodies in metastatic melanoma. Annals of oncology : official journal of the European Society for Medical Oncology / ESMO. 2017;28(5):1130–6. doi: 10.1093/annonc/mdx026.

32. Guibert N, Mazieres J, Delaunay M, Casanova A, Farella M, Keller L, et al. Monitoring of KRAS-mutated ctDNA to discriminate pseudo-progression from true progression during anti-PD-1 treatment of lung adenocarcinoma. Oncotarget. 2017;8(23):38056–60. doi: 10.18632/oncotarget.16935. [PubMed: 28445137]

33. Genovese G, Kahler AK, Handsaker RE, Lindberg J, Rose SA, Bakhoum SF, et al. Clonal hematopoiesis and blood-cancer risk inferred from blood DNA sequence. The New England journal of medicine. 2014;371(26):2477–87. doi: 10.1056/NEJMoa1409405. [PubMed: 25426838]

34. Steensma DP, Bejar R, Jaiswal S, Lindsley RC, Sekeres MA, Hasserjian RP, et al. Clonal hematopoiesis of indeterminate potential and its distinction from myelodysplastic syndromes. Blood. 2015;126(1):9–16. doi: 10.1182/blood-2015-03-631747. [PubMed: 25931582]

35. McNerney ME, Godley LA, Le Beau MM. Therapy-related myeloid neoplasms: when genetics and environment collide. Nature reviews. 2017;17(9):513–27. doi: 10.1038/nrc.2017.60.

36. Tumeh PC, Harview CL, Yearley JH, Shintaku IP, Taylor EJ, Robert L, et al. PD-1 blockade induces responses by inhibiting adaptive immune resistance. Nature. 2014;515(7528):568–71. doi: 10.1038/nature13954. [PubMed: 25428505]

37. Subudhi SK, Aparicio A, Gao J, Zurita AJ, Araujo JC, Logothetis CJ, et al. Clonal expansion of CD8 T cells in the systemic circulation precedes development of ipilimumab-induced toxicities. Proceedings of the National Academy of Sciences of the United States of America. 2016;113(42):11919–24. doi: 10.1073/pnas.1611421113. [PubMed: 27698113]

Statement of Significance

Rapid and sensitive detection of circulating tumor DNA dynamic changes and T cell expansion can be used to guide immune targeted therapy for patients with lung cancer.

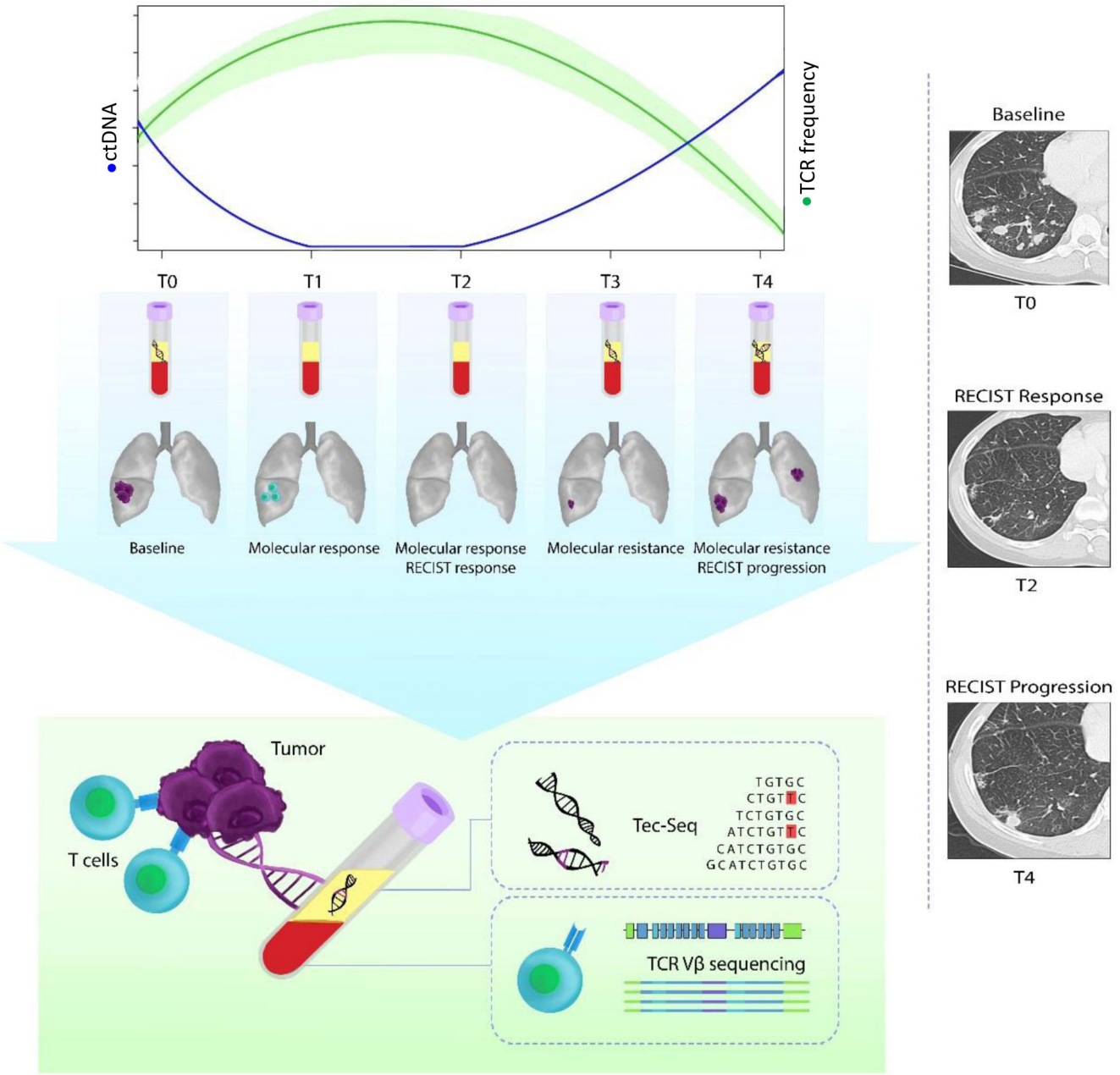

Figure 1. Overview of next-generation sequencing and T cell analyses.

We used serial blood samples collected at baseline, early after treatment initiation and at additional timepoints during immune checkpoint blockade to determine ctDNA and TCR repertoire dynamics. ctDNA trends were evaluated by TEC-Seq and the evolving TCR repertoire was assessed by TCR next generation sequencing. Dynamic changes in ctDNA and TCR clonotypic expansions were used to identify molecular response patterns and compared to RECIST 1.1 tumor burden evaluations. T0–T4 denote serial timepoints from the time of treatment initiation (T0), to the time of molecular response (T1), radiologic response (T2), molecular resistance (T3) and radiologic progression (T4).

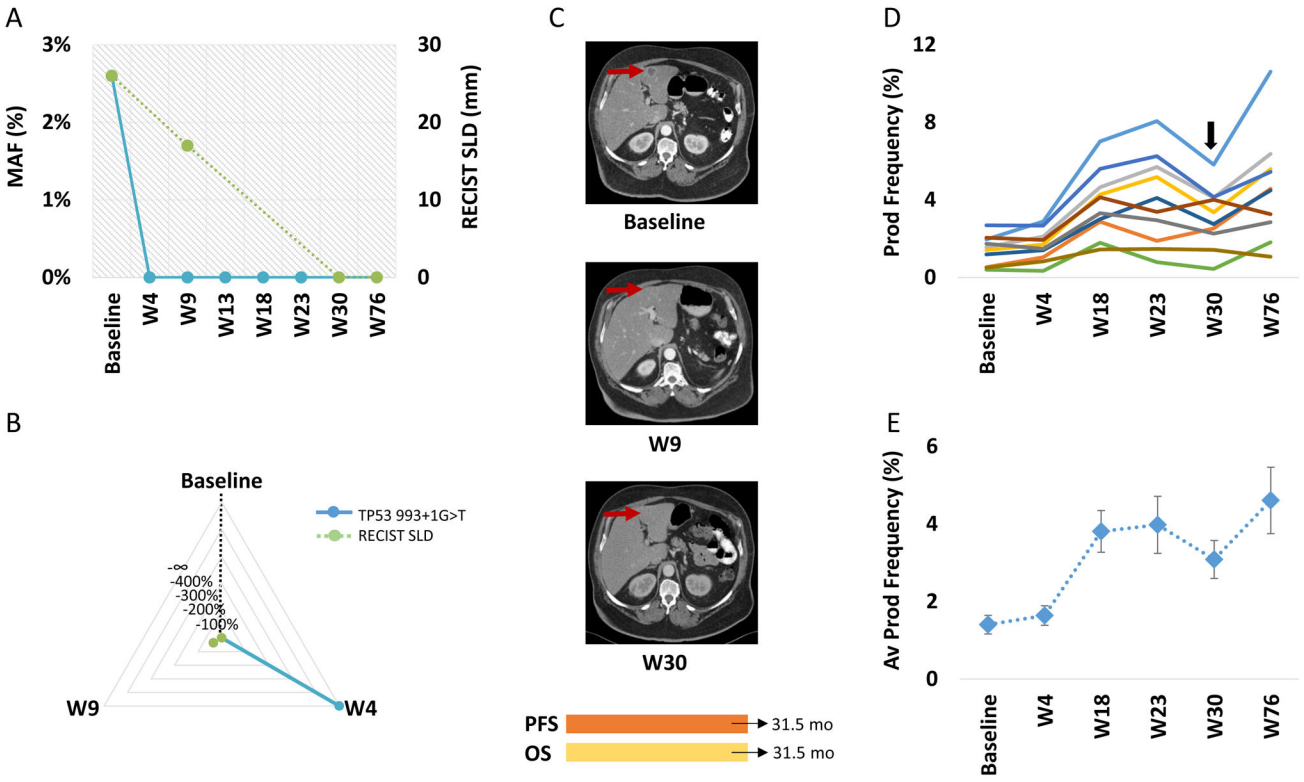

Figure 2. ctDNA and TCR clonal dynamics for a patient with sustained response to anti-PD1.

ctDNA (TP53 993+1G>T mutation shown in blue) decreased to undetectable levels signifying a complete molecular response at week 4 (**A**), in contrast CT imaging did not accurately capture the rate (**B**) or timing (**C**) of tumor regression (RECIST tumor burden dynamics are shown in green). A complete response by RECIST 1.1 was achieved 26 weeks later than the molecular response **(C)**. In parallel, TCR repertoire dynamics revealed clonotypic amplifications of intratumoral TCR clones in peripheral blood at the time of radiographic response. TCR clones with statistically significant differential abundance were evaluated as individual clones (**D**) and as a composite of productive frequencies (**E**). Patient was off anti-PD1 therapy and on immunosuppressive therapy at week 30 (arrow), due to emergence of immune-related toxicity.

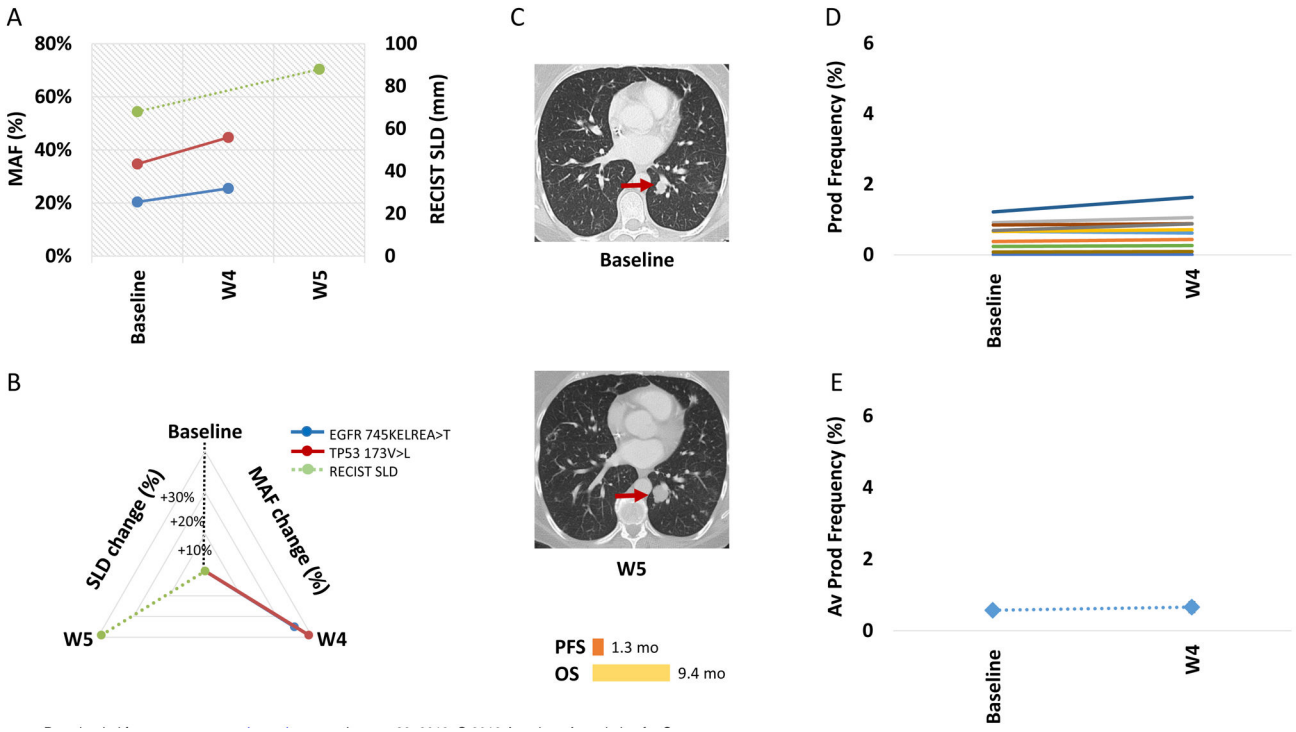

Figure 3. ctDNA and TCR clonal dynamics for a patient with primary resistance to anti-PD1.

ctDNA levels (EGFR 745KELREA>T and TP53173V>L mutations shown in blue and red respectively) continued to rise from the time of initiation of anti-PD1 therapy (**A**). For this patient the change in the RECIST tumor burden was similar to the increase in ctDNA levels (RECIST tumor burden dynamics shown in green, **B**), however molecular resistance was detected earlier than conventional CT imaging (**C**). There were no clones with statistically significant expansion at week 4 compared to baseline, top 10 intratumoral clones found in peripheral blood are shown as individual clones (**D**) and by their average productive frequency (**E**).

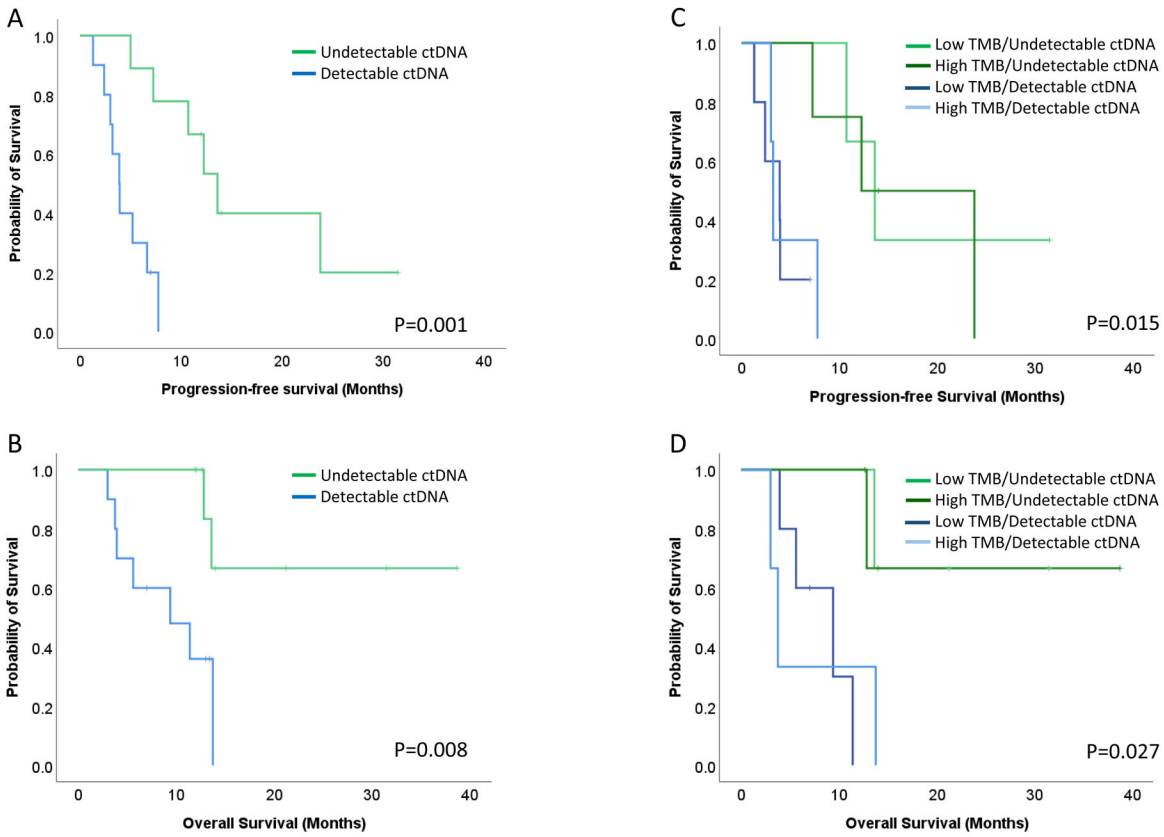

Figure 4. Early ctDNA clearance predicts progression-free and overall survival.

Patients with reduction of ctDNA to undetectable levels demonstrated a significantly longer PFS and OS compared to patients with no evidence of ctDNA elimination (log rank p=0.001 and P=0.008 respectively, **A** and **B**). Patients with undetectable ctDNA (molecular responders) clustered together independent of their tumor mutation burden (**C**) and the same pattern was observed for patients with detectable ctDNA (molecular nonresponders, **D**). Patients with ctDNA molecular response and either high or low tumor mutation burden had a significantly longer progression-free and overall survival (log rank P=0.015 and P=0.027 respectively).

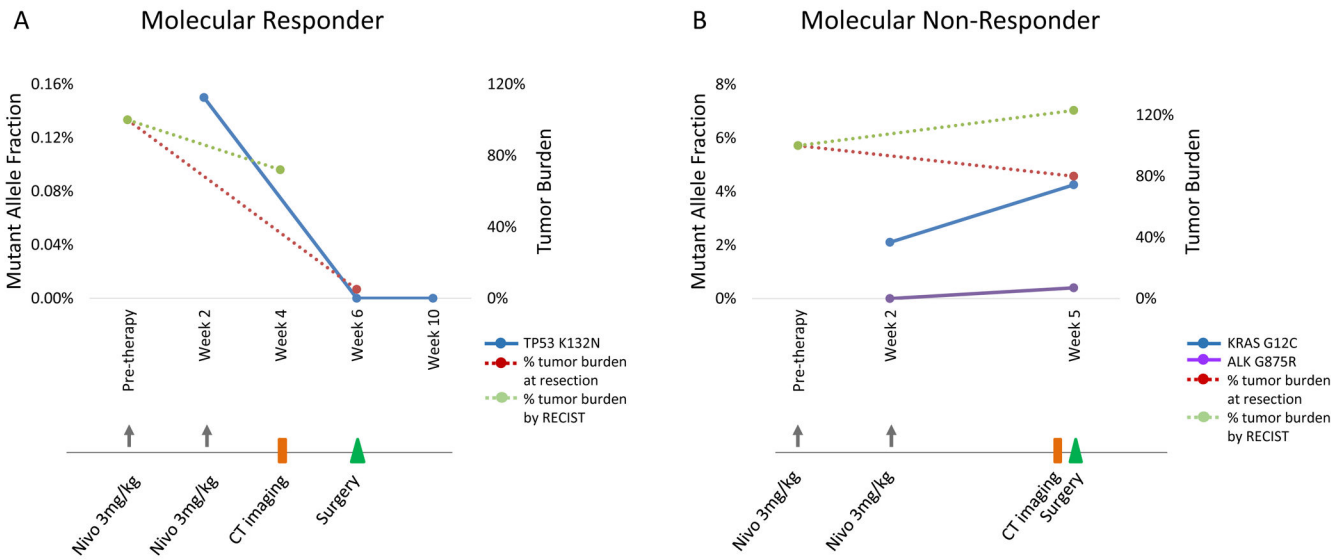

Figure 5. Early ctDNA clearance is associated with pathologic response to anti-PD1 therapy.

Molecular responses were consistent with pathologic responses to anti-PD1 therapy in early stage NSCLC. For a patient with a major pathologic response, ctDNA elimination (TP53 K132N mutation shown in blue) accurately captured the therapeutic effect compared to RECIST tumor burden dynamics (shown in green) that showed stable disease (**A**). In contrast, ctDNA levels (KRAS G12C and ALK G875R mutations shown in blue and purple) increased from baseline for a patient that did not achieve a pathologic response to anti-PD1 therapy (**B**). Changes in RECIST tumor burden, shown on the secondary axis of each plot, did not accurately predict outcome as both patients were classified as stable disease. The timeline of anti-PD1 therapy dosing, radiographic assessments and tumor resection is shown below each graph.

Table 1.

Summary of clinical and molecular characteristics

Patient	Immune-targeted therapy	Metastatic vs. Early Stage	Progression-free Survival (0 - Progression-free; 1 - Progression)	PFS (months)	Overall Survival (0-censored; 1-Dead of disease)	OS (months)	Number of tumor-specific variants at baseline	ctDNA molecular response (0=no, 1=yes)	Clonal TCR expansion (0=no, l=yes)	Tumor Mutation Burden
Metastatic NSCLC (N=24)										
CGLU111	nivolumab	IV	0	N/A	0	31.5	1	1	1	174
CGLU115	nivolumab	IV	1	3.2	1	3.8	1	0	0	285
CGLU121	nivolumab	IV	1	1.3	1	9.4	1	0	0	68
CGLU159	nivolumab	IV	1	3.9	1	5.6	1	0	1	65
CGLU160	nivolumab	IV	1	13.6	1	13.6	1	1	N/A	50
CGLU161	nivolumab-ipilimumab	IV	1	8.6	1	13.2	0	ND	1	127
CGLU162	nivolumab	IV	0	7.0	0	7.0	3	0	0	169
CGLU168	nivolumab	IV	1	7.3	0	12.6	1	1	N/A	411
CGLU203	nivolumab	IV	1	3.9	1	3.9	1	0	1	90
CGLU211	nivolumab	IV	1	10.7	0	21.3	1	1	N/A	161
CGLU212	nivolumab	IV	1	12.3	1	12.8	2	1	1	368
CGLU135	nivolumab	IV	1	23.8	0	38.7	1	1	1	358
CGLU127	nivolumab	IV	1	9.9	1	25.4	N/A	N/A	1	335
CGLU117	nivolumab	IV	1	7.8	1	13.8	3	0	1	296
CGLU243	nivolumab	IV	1	2.4	1	11.4	2	0	1	42
CGLU329	pembrolizumab	IV	0	14.0	0	14.0	0	ND	N/A	91
CGLU337	pembrolizumab-chemotherapy	IV	0	14.0	0	14.0	4	1	N/A	846
CGLU340	nivo-anti-LAG3	IV	1	6.6	0	13.4	1*	0	N/A	N/A*
CGLU341	pembrolizumab-chemotherapy	IV	0	13.0	0	13.0	0	ND	N/A	624
CGLU347	pembrolizumab	IV	1	5.0	0	12.0	1*	1	N/A	N/A*
CGLU348	pembrolizumab	IV	1	3.0	1	3.0	2	0	N/A	191
CGLU357	pembrolizumab	IV	1	5.2	0	13.0	1*	0	N/A	N/A*
CGLU351	pembrolizumab	IV	0	12.0	0	12.0	1*	1	N/A	N/A*
CGU368	pembrolizumab-chemotherapy	IV	0	12.0	0	12.0	0	ND	N/A	N/A*

Patient	Immune-targeted therapy	Metastatic vs. Early Stage	Progression-free Survival (0 - Progression-free; 1 - Progression)	PFS (months)	Overall Survival (0-censored; 1-Dead of disease)	OS (months)	Number of tumor-specific variants at baseline	ctDNA molecular response (0=no, 1=yes)	Clonal TCR expansion (0=no, l=yes)	Tumor Mutation Burden
Early Stage NSCLC (N=14)										
CGLU204	nivolumab	IIA	0	20	0	20.0	0	ND	N/A	N/A **
CGLU205	nivolumab	IIIA	0	30	0	30	1	1	N/A	99
CGLU206	nivolumab	IB	0	23	0	23	1	1	N/A	N/A **
CGLU215	nivolumab	IA	0	3	0	3	0	ND	N/A	310
CGLU217	nivolumab	IIIA	1	14	0	14	0	ND	N/A	68
CGLU218	nivolumab	IB	0	17	0	17	0	ND	N/A	5
CGLU219	nivolumab	IIIA	0	2	0	2	1	1	N/A	N/A **
CGLU220	nivolumab	IIIA	0	17	0	17	0	ND	N/A	26
CGLU221	nivolumab	IIA	0	N/A	0	28	1	1	N/A	190
CGLU222	nivolumab	IIA	1	3	0	28	2	0	N/A	75
CGLU224	nivolumab	IB	0	11	0	11	0	ND	N/A	105
CGLU225	nivolumab	IIIA	0	15	0	15	2	0	N/A	N/A **
CGLU249	nivolumab	IIB	0	8	0	8	1	1	N/A	N/A **
CGLU279	nivolumab	IIB	0	12	0	12	0	ND	N/A	N/A **

Major pathologic response (MPR) was defined as ≤10% viable tumor cells at the time of surgical resection (Forde et al., NEJM, 2018).

* exome sequencing was not performed; for these cases CLIA-targeted NGS was performed for clinical purposes

** the baseline tumor was not available for whole exome sequencing, the resection sample was analyzed and used to identify tumor-specific variants in ctDNA. TCR expansion was. assessed at the time of radiographic response. PFS; progression-free survival, OS; overall survival, ND; not detected, N/A; not evaluable,